Research Article | Vol. 25, No. 22 | 30 Oct 2017 | OPTICS EXPRESS 27431
Optics EXPRESS

Germanium-on-silicon waveguides operating at mid-infrared wavelengths up to 8.5 μm

MILOS NEDELJKOVIC,[1,*] JORDI SOLER PENADES,[1] VINITA MITTAL,[1] GANAPATHY SENTHIL MURUGAN,[1] ALI Z. KHOKHAR,[1] CALLUM LITTLEJOHNS,[1,2] LEWIS G. CARPENTER,[1] CORIN B. E. GAWITH,[1] JAMES S. WILKINSON,[1] AND GORAN Z. MASHANOVICH[1,3]

[1] *Optoelectronics Research Centre, University of Southampton, Southampton, Hampshire, SO17 1BJ, UK*
[2] *Silicon Technologies Centre of Excellence, Department of Electronic and Electrical Engineering, Nanyang Technological University, Singapore, 639798, Singapore*
[3] *School of Electrical Engineering, University of Belgrade, 11120 Belgrade, Serbia*
[*] *m.nedeljkovic@soton.ac.uk*

Abstract: We report transmission measurements of germanium on silicon waveguides in the 7.5-8.5 μm wavelength range, with a minimum propagation loss of 2.5 dB/cm at 7.575 μm. However, we find an unexpected strongly increasing loss at higher wavelengths, potential causes of which we discuss in detail. We also demonstrate the first germanium on silicon multimode interferometers operating in this range, as well as grating couplers optimized for measurement using a long wavelength infrared camera. Finally, we use an implementation of the "cut-back" method for loss measurements that allows simultaneous transmission measurement through multiple waveguides of different lengths, and we use dicing in the ductile regime for fast and reproducible high quality optical waveguide end-facet preparation.

OCIS codes: (130.0130) Integrated optics, (040.3060) Infrared, (130.5990) Semiconductors.

References and links

1. G. Z. Mashanovich, F. Y. Gardes, D. J. Thomson, Y. Hu, L. Ke, M. Nedeljkovic, J. Soler Penades, A. Z. Khokhar, C. J. Mitchell, S. Stankovic, R. Topley, S. A. Reynolds, W. Yun, B. Troia, V. M. N. Passaro, C. G. Littlejohns, T. Dominguez Bucio, P. R. Wilson, and G. T. Reed, "Silicon Photonic Waveguides and Devices for Near- and Mid-IR Applications," IEEE J. Sel. Top. Quantum Electron. **21**, 1–12 (2015).
2. A. Spott, Y. Liu, T. Baehr-Jones, R. Ilic, and M. Hochberg, "Silicon waveguides and ring resonators at 5.5μm," Appl. Phys. Lett. **97**, 213501 (2010).
3. F. Li, S. D. Jackson, C. Grillet, E. Magi, D. Hudson, S. J. Madden, Y. Moghe, C. O'Brien, A. Read, S. G. Duvall, P. Atanackovic, B. J. Eggleton, and D. J. Moss, "Low propagation loss silicon-on-sapphire waveguides for the mid-infrared," Opt. Express **19**, 15212–15220 (2011).
4. S. Khan, J. Chiles, J. Ma, and S. Fathpour, "Silicon-on-nitride waveguides for mid- and near-infrared integrated photonics," Appl. Phys. Lett. **102**, 121104 (2013).
5. A. Spott, J. Peters, M. L. Davenport, E. J. Stanton, C. D. Merritt, W. W. Bewley, I. Vurgaftman, C. S. Kim, J. R. Meyer, J. Kirch, L. J. Mawst, D. Botez, and J. E. Bowers, "Quantum cascade laser on silicon," Optica **3**, 545 (2016).
6. J. S. Penades, A. Ortega-Moñux, M. Nedeljkovic, J. G. Wangüemert-Pérez, R. Halir, A. Z. Khokhar, C. Alonso-Ramos, Z. Qu, I. Molina-Fernández, P. Cheben, and G. Z. Mashanovich, "Suspended silicon mid-infrared waveguide devices with subwavelength grating metamaterial cladding," Opt. Express **24**, 22908 (2016).
7. R. Soref, "Mid-infrared photonics in silicon and germanium," Nature Photon. **4**, 495–497 (2010).
8. M. Brun, P. Labeye, G. Grand, J.-M. Hartmann, F. Boulila, M. Carras, and S. Nicoletti, "Low loss sige graded index waveguides for mid-ir applications," Opt. Express **22**, 508–518 (2014).
9. M. Nedeljkovic, J. S. Penades, C. J. Mitchell, A. Z. Khokhar, S. Stankovic, T. D. Bucio, C. G. Littlejohns, F. Y. Gardes, and G. Z. Mashanovich, "Surface-Grating-Coupled Low-Loss Ge-on-Si Rib Waveguides and Multimode Interferometers," IEEE Photon. Technol. Lett. **27**, 1040–1043 (2015).
10. Y.-C. Chang, V. Paeder, L. Hvozdara, J.-M. Hartmann, and H. P. Herzig, "Low-loss germanium strip waveguides on silicon for the mid-infrared," Opt. Lett. **37**, 2883–2885 (2012).
11. G. Z. Mashanovich, C. J. Mitchell, J. S. Penades, A. Z. Khokhar, C. G. Littlejohns, W. Cao, Z. Qu, S. Stanković, F. Y. Gardes, T. B. Masaud, H. M. H. Chong, V. Mittal, G. S. Murugan, J. S. Wilkinson, A. C. Peacock, and M. Nedeljkovic,

#302579 https://doi.org/10.1364/OE.25.027431
Journal © 2017 Received 17 Jul 2017; revised 14 Sep 2017; accepted 14 Sep 2017; published 24 Oct 2017

Optics EXPRESS

"Germanium mid-infrared photonic devices," J. Lightwave Technol. **35**, 624–630 (2017).
12. Tydex, "Tydex Germanium data sheet," http://www.tydexoptics.com/pdf/Germanium.pdf.
13. Tydex, "Tydex Silicon data sheet," http://www.tydexoptics.com/pdf/Si.pdf.
14. C. Alonso-Ramos, A. Ortega-Moñux, I. Molina-Fernández, P. Cheben, L. Zavargo-Peche, and R. Halir, "Efficient fiber-to-chip grating coupler for micrometric SOI rib waveguides," Opt. Express **18**, 15189 (2010).
15. J. Favreau, C. Durantin, J.-M. Fédéli, S. Boutami, and G.-H. Duan, "Suspended mid-infrared fiber-to-chip grating couplers for SiGe waveguides," Proc. SPIE **9753**, 975319 (2016).
16. D. J. Thomson, Y. Hu, G. T. Reed, and J. M. Fedeli, "Low Loss MMI Couplers for High Performance MZI Modulators," IEEE Photon. Technol. Lett. **22**, 1485–1487 (2010).
17. M. Nedeljkovic, S. Stankovic, C. J. Mitchell, A. Z. Khokhar, S. A. Reynolds, D. J. Thomson, F. Y. Gardes, C. G. Littlejohns, G. T. Reed, and G. Z. Mashanovich, "Mid-infrared thermo-optic modulators in SoI," IEEE Photon. Technol. Lett. **26**, 1352–1355 (2014).
18. L. Soldano and E. Pennings, "Optical multi-mode interference devices based on self-imaging: principles and applications," J. Lightwave Technol. **13**, 615–627 (1995).
19. T. G. Bifano, T. A. Dow, and R. O. Scattergood, "Ductile-regime grinding: a new technology for machining brittle materials," J. Eng. Industry **113**, 184 (1991).
20. L. G. Carpenter, H. L. Rogers, P. A. Cooper, C. Holmes, J. C. Gates, and P. G. R. Smith, "Low optical-loss facet preparation for silica-on-silicon photonics using the ductile dicing regime," J. Phys. D: Appl. Phys. **46**, 475103 (2013).
21. K. Mizuuchi, T. Sugita, K. Yamamoto, T. Kawaguchi, T. Yoshino, and M. Imaeda, "Efficient 340-nm light generation by a ridge-type waveguide in a first-order periodically poled MgO:$LiNbO_3$," Opt. Lett. **28**, 1344 (2003).
22. V. Mittal, A. Aghajani, L. G. Carpenter, J. C. Gates, J. Butement, P. G. R. Smith, J. S. Wilkinson, and G. S. Murugan, "Fabrication and characterization of high-contrast mid-infrared $GeTe_4$ channel waveguides," Opt. Lett. **40**, 2016 (2015).
23. M. F. Volk, S. Suntsov, C. E. Rüter, and D. Kip, "Low loss ridge waveguides in lithium niobate thin films by optical grade diamond blade dicing," Opt. Express **24**, 1386 (2016).
24. F. Grillot, L. Vivien, S. Laval, and E. Cassan, "Propagation loss in single-mode ultrasmall square silicon-on-insulator optical waveguides," J. Lightwave Technol. **24**, 891 (2006).
25. S. Sakaguchi and S.-i. Todoroki, "Optical properties of GeO_2 glass and optical fibers," Appl. Opt. **36**, 6809 (1997).
26. R. Kurstjens, K. Dessein, and C. Quaeyhaegens, "Shelf life for ge wafers," Proceedings of 10th European Space Power Conference : 13-17 April 2014 Noordwijkerhout, the Netherlands (2014).
27. E. Artacho, F. Ynduráin, B. Pajot, R. Ramírez, C. P. Herrero, L. I. Khirunenko, K. M. Itoh, and E. E. Haller, "Interstitial oxygen in germanium and silicon," Phys. Rev. B **56**, 3820–3833 (1997).
28. F. A. Johnson, "Lattice absorption bands in silicon," Proc. Phys. Soc. **73**, 265 (1959).
29. S. J. Fray, F. A. Johnson, J. E. Quarrington, and N. Williams, "Lattice bands in germanium," Proc. Phys. Soc. **85**, 153 (1965).
30. M. Nedeljkovic, R. Soref, and G. Z. Mashanovich, "Predictions of free-carrier electroabsorption and electrorefraction in germanium," IEEE Photon. J. **7**, 1–14 (2015).
31. D. B. Cuttriss, "Relation between surface concentration and average conductivity in diffused layers in germanium," Bell System Tech. J. **40**, 509–521 (1961).

1. Introduction

The mid-infrared (MIR) wavelength range is fundamentally interesting for a wide variety of sensing applications, because many gases and chemicals exhibit strong absorption lines in this region, and particularly in the so-called "fingerprint range" (8-14 μm). In recent years there has been great progress in the development of group-IV material photonic waveguide platforms that operate in the MIR. Firstly, several waveguide platforms which use a Si waveguide core and different lower cladding materials have been demonstrated: silicon-on-insulator (SOI) has been demonstrated up to 3.8 μm wavelengths [1], beyond which SiO_2 absorption becomes prohibitive; silicon-on-sapphire (SOS) has been demonstrated up to 5.5 μm [2] (and is expected to be transparent up to 7 μm [3]); in silicon on silicon nitride low loss waveguiding has been shown at 3.39 μm in [4] and quantum cascade laser integration has been demonstrated at 4.8 μm [5]; and suspended silicon waveguides, which are expected to be able to exploit the full Si MIR transparency range (up to 8.5 μm) have been demonstrated up to 3.8 μm wavelength [6]. SiGe graded index and Germanium on silicon (Ge-on-Si) material platforms have been proposed for use at longer wavelengths at which Si absorption is too high for its use as a waveguide core material [7]. SiGe waveguides have been demonstrated with a loss of only 2.0 dB/cm at 7.4

Optics EXPRESS

μm [8], showing that they can be used at least throughout the whole Si transparency range. Because SiGe waveguides contain a mixture of Si and Ge, the Ge-on-Si platform with a fully Ge core would be expected to be transparent over an even wider range. To date Ge-on-Si waveguides with a loss of only 0.6 dB/cm have been demonstrated at 3.8 μm [9], and have been used at 5.8 μm with a loss of < 2.5 dB/cm [10], and at 7.5 μm with a loss of 3.0±0.8 dB/cm [11].

In this paper we extend the use of Ge-on-Si waveguides up to the 7.5-8.5 μm range. We also present in detail an implementation of the "cut-back" method for propagation loss measurement that makes use of 1x2 multimode interferometers (MMIs) and grating couplers, which could be used more generally for rapid planar photonic waveguide loss characterization, and we use dicing for high quality Ge-on-Si waveguide facet preparation for the first time. The loss measurements in this range raise new questions about absorption mechanisms in Ge-on-Si in the 8-14 μm range, which we discuss in detail.

2. Experimental setup and measurement design

The experimental apparatus used for waveguide transmission measurement consisted of a tunable quantum cascade laser (Pranalytica Inc.), which was focused with a ZnSe objective lens into a single mode As_2Se_3 fiber with a fiber core diameter of 12 μm (IRflex). The laser operates in a pulsed, quasi-continuous wave mode, with an average output power of 135 mW at 7.5 μm and 40 mW at 8.5 μm. At the output of the input fiber the power was measured to be 17.5 mW at 7.5 μm and 0.3 mW at 8.5 μm. A long-wavelength infrared (LWIR) camera (FLIR SC660) was mounted to look over the waveguide chip from above. At the output another fibre leading to a TE cooled HgCdTe detector (Vigo Systems) was used for collecting the transmitted light.

In a first attempt at demonstrating waveguide transmission and measuring Ge-on-Si waveguide losses in the 7.5-9 μm range, Ge-on-Si waveguide chips that could be measured by fibre butt coupling were designed and fabricated (described fully in sections 3 and 4). The waveguides tapered out to 30 μm width at the facets, and the chip facets were prepared by cleaving. Initially a fibre was butt coupled to the waveguide input facet, and the LWIR camera positioned above the chip was used to observe light at the waveguide output facet, thus confirming waveguiding. A second fibre, leading to the detector, was then butt coupled to the output facet. However, in this configuration no detector response corresponding to the waveguide transmission was measured, which was believed to be due to high coupling losses arising from mismatch of the fibre and tapered waveguide modes.

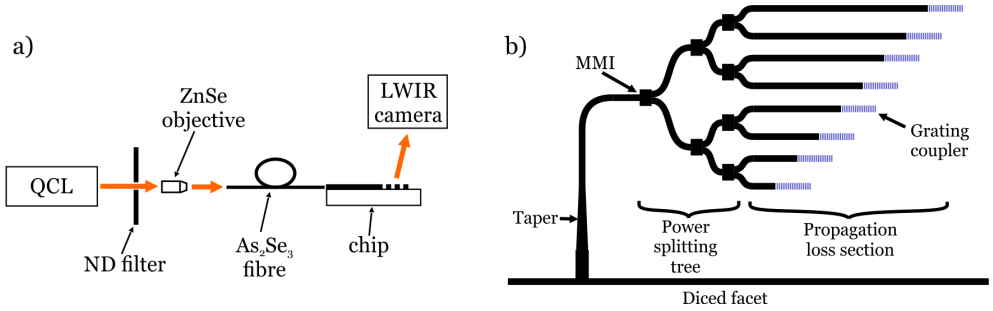

Fig. 1. a) Schematic diagram of the lateral view of the experimental setup. b) Schematic diagram of the photonic "cut-back" circuit for waveguide propagation loss measurement. Figure reprinted with permission from [11].

The measurement approach was therefore adapted to instead use the LWIR camera for detection, since the camera read-out pixel values are proportional to the optical power intensity: a fiber was used for input coupling, but grating couplers were placed at waveguide outputs to direct light

Optics EXPRESS

out of the plane of the chip up towards the camera, as shown in Fig. 1(a). This measurement method was previously used in [11]. Using this alternative configuration provided an opportunity to simultaneously measure the transmissions through multiple waveguides and grating couplers. A 1x8 splitting tree (employing 1x2 MMIs as splitters) was designed to split the light into 8 waveguides, and an effective cut-back loss measurement circuit was designed in which the splitting tree lead to an array of waveguides of different lengths, each with a grating coupler at its output, as shown in Fig. 1(b). Using this method accelerates measurements, removes the need to have identical facets at the end of each waveguide, and reduces the requirement for perfect alignment between the fibre and waveguide. Due to their symmetry 1x2 MMIs theoretically have perfectly even splitting ratios, and are tolerant to fabrication imperfections. Grating couplers fabricated by lithography would also be expected to be more tolerant of fabrication variation than waveguide facets.

To measure the light transmission through a grating coupler as observed by the camera, a background image is first captured with the laser off (Image 0), followed by an identical image with the laser on (Image 1), then Image 0 is subtracted from Image 1 to correct for the background. The pixel intensities of a rectangular area surrounding the grating coupler are then summed together, producing a single value that is proportional to the grating coupler transmission.

The design of each of the elements making up this circuit are discussed in detail in section 3.

3. Device design and simulation

3.1. Waveguides

The waveguides were designed to be fabricated on Ge-on-Si wafers with a 3 μm thick Ge layer and etch depth of 1.8 μm, that is, for the same platform that we previously used to demonstrate low loss waveguides at the wavelength $\lambda = 3.8\mu$m [9]. Waveguides were simulated using the Eigenmode solver in Lumerical Mode Solutions software. In fact our simulations, which took into account only material losses from pure crystalline Ge and Si [12, 13], showed that single mode waveguides supporting TE polarization could be designed for this same Ge thickness and etch depth for the whole transparency range of Ge ($\lambda = 2 - 16$ μm), requiring only that the waveguide width be tailored to the wavelength. Figure 2 shows the simulated waveguide width at which the 1st higher order TE mode appears, as well as the expected propagation loss corresponding to that waveguide width, for wavelengths across the 2-16 μm range. A width (W) = 4.3 μm was chosen for single mode propagation at $\lambda = 7.5 - 9.0$ μm. We also simulated that etching a 9 μm wide region alongside the waveguide would be sufficient to suppress any lateral leakage from the waveguide. The 90° bend in the access waveguide had a radius of 300 μm.

3.2. Grating couplers

In silicon photonics grating couplers are conventionally used to couple light between waveguides and fibres, and the grating coupler dimensions are designed to minimize coupling losses by optimizing the overlap between the light radiated by the grating coupler and the mode supported by the fibre. However, if a camera is used to collect the light the design requirements are simplified; light radiated upwards by the grating coupler should be maximized, and the light being reflected back into the waveguide should be minimized (to prevent Fabry-Perot ripples in the transmission spectrum). In addition, the effective grating coupler bandwidth can be improved, because as the wavelength changes the radiation angle of the diffracted light changes, and the camera is able to accept light radiated over a much wider range of angles than a fibre placed above the grating.

We also note that an issue with the Ge-on-Si platform is that because of the high Ge-air refractive index mismatch, the effective index of the Bloch mode propagating in the grating region is very different to that of the Ge access waveguide mode [14, 15], therefore a high contrast grating is likely accompanied by large back-reflections.

Optics EXPRESS

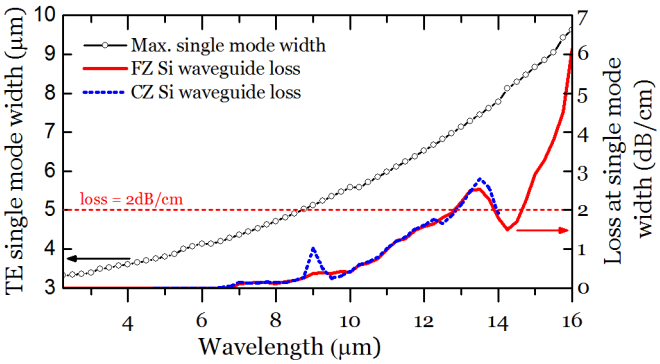

Fig. 2. Black line with circles shows for different wavelengths the simulated waveguide width at which the 1^{st} higher order TE mode appears, in a Ge-on-Si waveguide with height 3 μm and etch depth 1.8 μm at different wavelengths. The solid line (red) shows the simulated propagation loss for a waveguide at that same width and wavelength, with a Float Zone (FZ) Si substrate. The dotted line (blue) shows the simulated propagation loss for a waveguide at that same width and wavelength, but with a Czhochralski (CZ) Si substrate. The loss values only include loss coming from bulk material absorption of Ge and Si.

The side-benefit of using a camera for light collection in this case is that we can instead design weak, but long, grating couplers, which over their length have high total upwards radiated power and low reflection. The grating couplers were designed to have an etch depth of 1.0 μm, a period of 2.0 μm, a duty cycle of 0.7, and to be 400 μm long and 35 μm wide. Figure 3(a) shows the simulated upwards radiation and reflection of the grating over the wavelength range 7.5-9.0 μm (2D simulations were conducted using Lumerical FDTD software). Figure 3(b) shows a scanning electron microscope (SEM) image of one of the fabricated grating couplers.

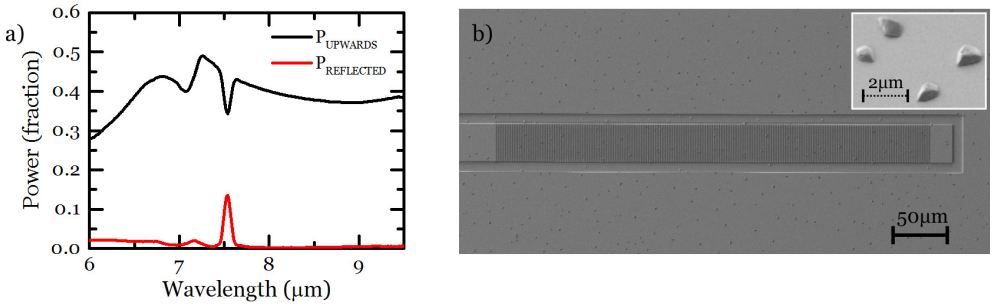

Fig. 3. a) Simulated grating coupler response for 400 μm long grating with etch depth 1.0 μm, period = 2.0 μm and duty cycle = 0.7, showing fractions of power radiated upwards and reflected back into the access waveguide, for λ = 6.0-9.5 μm. b) Scanning electron microscope image of a fabricated grating coupler. The inset shows an expanded view of several of the time dependent haze defects that appear on the Ge surface over time.

3.3. *Multimode interferometers and splitting tree*

MMIs were used as the 1x2 splitters in the splitting tree because of their known tolerance to fabrication imperfections [16]. They were designed according to the process previously described in [16, 17]. We note that from multi-mode self-imaging theory [18], as the wavelength is increased the self-imaging length in the MMI decreases, but that due to the necessarily larger mode

Optics EXPRESS

width the output ports must be separated further to prevent evanescent coupling between them. Therefore the multimode region must also be widened, which brings an accompanying length increase. Following simulations in Photon Design Fimmprop software we chose the following MMI dimensions: the multimode region was 20 μm wide and 91.4 μm long, the output ports had a centre-to-centre spacing of 10.3 μm, and the input and output ports were tapered from the single mode waveguide width out to a maximum width of 9.7 μm, over a 100 μm length. The simulations predicted that over the wavelength range 7.5-9.0 μm these splitters would have an individual insertion loss of 0.07-0.19 dB.

In the splitting tree S-bends were used to further separate the outputs of the MMIs. Following the three 1x2 splitter stages, the S-bends had lengths 1500 μm, 750 μm, and 350 μm, and lateral offsets 595 μm, 295 μm, and 145 μm, respectively.

4. Fabrication

The devices were fabricated using the same 3 μm thick Ge-on-Si material that we previously used to demonstrate low loss waveguides at the 3.8 μm wavelength [9]. At the time we showed that the Ge was crystalline with the majority of defects being confined to an approximately 200 nm thick region at the Ge/Si interface. We used the same lithography and etching processes as were previously described: E-beam lithography with ZEP520 resist was used for patterning, while ICP etching with SF_6 and C_4F_8 gases transferred the pattern into the Ge layer. The grating couplers were first etched to a depth of 1.0 μm, then the waveguides were etched 1.8 μm.

In our early experiments the waveguide facets were prepared by cleaving with a diamond scribe, but this was found to be inconsistent, therefore we investigated facet preparation through chip dicing. Dicing is a mechanical sawing technique often used in the semiconductor industry to separate dies/chips from wafers. Typically, dicing is optimized for speed and throughput while cutting dies. However, cut quality can be greatly improved if ductile regime machining at a material's plastic limit is achieved [19]. By machining in the ductile regime, high quality, optical grade surfaces can be produced with vertical sidewalls and nanoscale surface roughness [20]. This technique employs stringent machining parameters for blade grit size and grit concentration, blade rotational speed, sample translation speed, depth of cut, and sample coolant; all must be optimised and maintained to sustain ductile machining. If machining strain exceeds the material's plastic limit, the more common brittle machining is initiated in which larger-scale surface roughness, cracking and chipping are caused at the cut sidewall.

Numerous groups have used dicing to produce optical quality surfaces, some of the first examples of which were in the production of periodically poled lithium niobate waveguides for second harmonic generation [21]. Waveguide facet preparation for optical-fibre butt coupling and free space optical launch have also been achieved via dicing, mitigating the need for laborious lapping and polishing. Various material platforms have used diced facets, including silica-on-silicon [20], germanium telluride-on-zinc selenide [22] and lithium niobate [23]. Facet surface roughnesses of 4.9 nm (Sa) and 3 nm (Sa) were achieved in silica-on-silicon [20] and germanium telluride-on-zinc selenide [22], respectively. Advantages of ductile dicing over lapping and polishing are speed, reduction in manual handling, and the ease with which composites with differential material hardness can be machined; hardness variation is common in composite integrated optics and can cause irregularities in lapped or polished surfaces.

For this work, Ge-on-Si waveguide facets were diced in the ductile regime; RMS and average surface roughnesses of 3.1 nm (Sa) and 3.9 nm (Sq) were achieved with a correlation length (1/e) of 1.2 μm. Roughness parameters were calculated using polynomial levelling for a 40 x 40 μm area including both the Ge waveguide and Si substrate. These waveguide facets were machined with the following dicing parameters: depth of cut of 50 μm, a blade rotational speed of 20 krpm, a translation speed of 0.1 mms^{-1} and using a nickel bonded diamond impregnated blade. The sample was also covered in S1813 photo resist and soft baked, providing a protective layer to

Optics EXPRESS

minimise topside chipping. Figure 4 shows a SEM image of a waveguide end facet that was diced in this way.

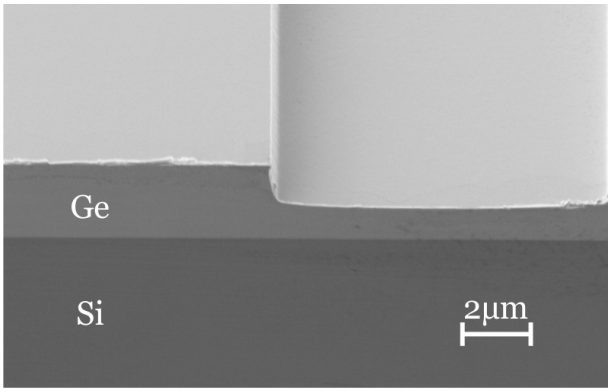

Fig. 4. Scanning electron microscope image of a diced waveguide facet.

5. Experimental measurements

Figure 5(a) shows an image captured by the LWIR camera when the laser light (tuned to the wavelength 7.825 μm) is coupled into the input waveguide. Figure 5(b) shows the same view, but when the background image (i.e. with the laser switched off) has been subtracted, and demonstrates clearly that light can be seen only at the grating couplers, and that the emitted light intensity decreases as the waveguide length increases. When the light was coupled to the loss measurement tree no light was visible at other identical grating couplers that were fabricated near to the devices under test, indicating that the observed light was coming from the waveguides, and was not simply uncoupled light that was being scattered by the gratings.

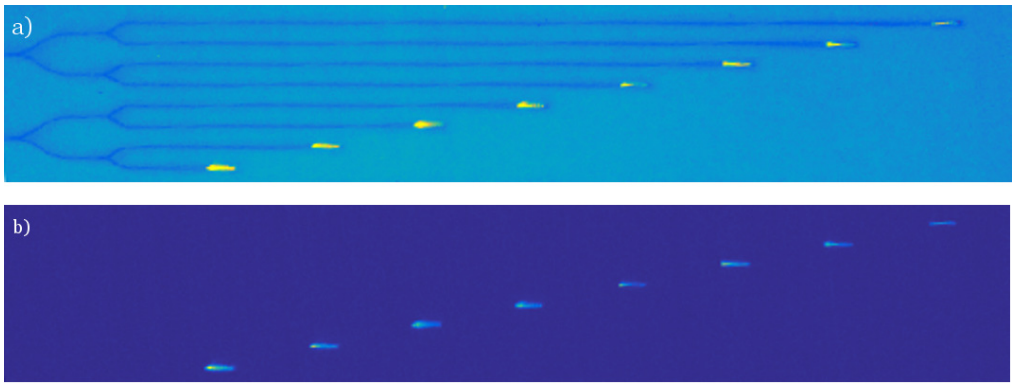

Fig. 5. a) Captured LWIR camera image with the QCL tuned to λ = 7.825 μm. Figure reprinted with permission from [11]. b) The same image, with the background image (i.e. when the laser is not emitting) subtracted.

Figure 6 (b) shows an example "cut-back loss" measurement graph for the waveguide transmission at a single wavelength (λ = 7.825 μm). The waveguide propagation loss is calculated from the gradient of the fitted line. Figure 6(a) shows the waveguide propagation loss, calculated using the same method, over the spectral range 7.5-8.5 μm. It can be seen that over this wavelength range the measured waveguide loss increases from 3.0 dB/cm (with a minimum of 2.5dB/cm

Optics EXPRESS

at 7.575 μm) to nearly 20 dB/cm. At wavelengths above 8.5 μm we were unable to measure waveguide transmission, which we attribute to the combined effects of the aforementioned high waveguide loss and also because of increasing input fibre absorption loss in this range. The increased scattering of the points above 8.0 μm is attributed to lower overall transmission at these wavelengths, which reduced the signal to noise ratio of the measurements. Section 6 discusses potential reasons for the measured waveguide loss.

The MMI loss was measured at $\lambda = 7.9$ μm by using the camera to measure relative transmission through separate waveguides containing different numbers of linked 1 x 2 MMIs. Figure 6(c) shows the cut-back loss data for this experiment. The length of the access waveguides to these test devices increased by 100 μm for each additional MMI that was introduced, therefore we used the propagation loss measured at this wavelength to adjust the transmission values. The measured insertion loss was 0.23±0.04 dB/MMI.

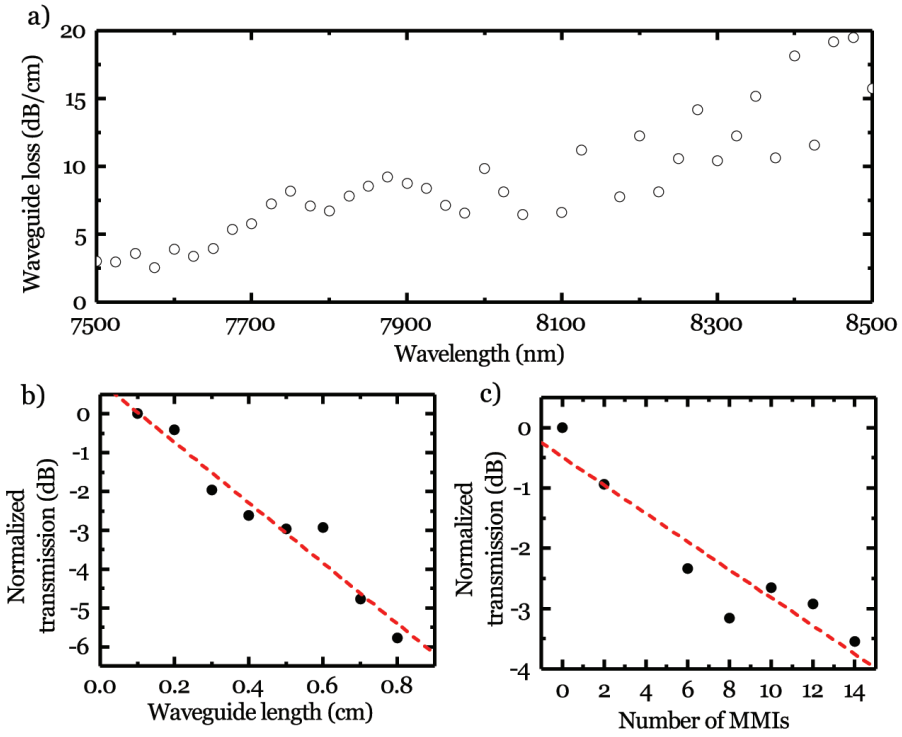

Fig. 6. a) Propagation loss (dB/cm) measured for Ge-on-Si waveguides at wavelengths between 7.5 and 8.5 μm. b) Effective cut-back loss measurement at a single wavelength, $\lambda = 7.825$ μm. The transmission is normalized to the transmission through the shortest waveguide. c) Multimode interferometer insertion loss measurement at $\lambda = 7.9$ μm, showing normalized transmission for chains of different numbers of MMIs. The insertion loss at this wavelength is 0.23±0.04 dB.

6. Discussion

It is clear that the waveguide loss difference across the measured spectral range is substantially higher than was initially predicted in our simulations by using the material loss data. A thorough experimental investigation of the various loss mechanisms that could be responsible is outside the scope of this work, but in this section we attempt to identify via literature survey possible

Optics EXPRESS

reasons for this excess loss, in order to guide further investigations into the effect. What follows is a list of potential sources of loss, and estimates of their effects:

a) *Silicon substrate absorption*: As previously noted, bulk Si absorption begins to increase above approximately 8 μm, which is predominantly due to multiphonon absorption. However, silicon substrate absorption in the LWIR region also depends on the interstitial oxygen and carbon impurity concentration in the material. Silicon wafers grown by the Czhochralski (CZ) method typically exhibit higher impurity levels and losses than those grown by the float zone (FZ) method. In our experiment the substrates were made from CZ type Si. We have incorporated absorption coefficient data for both FZ and CZ Si (calculated from wafer transmission data [13]), and have incorporated this data into our waveguide simulations. The simulated loss spectra for Ge-on-Si waveguides with both FZ and CZ type Si substrates are plotted in Fig. 2. This simulated loss is below 2 dB/cm up to approximately 13 μm. The CZ Si has an absorption peak at 9.0 μm, but we find that even at this peak the extra loss relative to that of FZ Si is <1dB/cm. These simulations therefore suggest that it is unlikely that Si substrate absorption is the most significant source of waveguide loss in the measured range.

b) *Sidewall roughness*: At near-infrared wavelengths scattering from sidewall roughness is the dominant loss mechanism in silicon waveguides. We have used the analytical equations presented in [24] to estimate the loss in the fundamental TE mode of Ge-on-Si waveguides with the fabricated dimensions from sidewall roughness scattering for wavelengths up to 9.0 μm. For this calculation we have assumed a very conservative r.m.s. roughness value of 50 nm, and have varied the correlation length from 50 nm to 400 nm. Mode simulations in Lumerical were used to estimate the waveguide mode effective index, which is required as an input to the analytical equations. Figure 7 shows calculation results.

   From theory Rayleigh scattering is proportional to λ^{-4}, and Fig. 7 showcases the consequences of this in stark terms. As the wavelength, mode size, and mode interaction with the sidewalls increase, at first the scattering loss also increases, but further increase of the wavelength reduces the scattering loss significantly. The maximum estimated loss in this range is around 0.30 dB/cm, and for every value of correlation length considered the scattering loss decreases from 7.5 μm to 8.5 μm. This analytical calculation indicates that sidewall scattering cannot be responsible for the large increase in experimental loss between 7.5 μm and 8.5 μm.

c) *Ge defects at Si interface:* We noted in [9] that in the Ge-on-Si wafers defects were apparent in the Ge material in the 200 nm thick Ge layer immediately adjacent to the Si interface, and that scattering at these defects was likely an important source of optical loss. Since in this experiment a much longer wavelength is used and the Ge thickness is the same, the mode overlap with this defect region is increased. However, the λ^{-4} dependence of Rayleigh scattering could be expected to mitigate this scattering loss, and does not agree with the increasing loss with increasing wavelength that is observed here. Nevertheless, these defects may exhibit states with wavelength dependent absorption features in this range.

d) *Native GeO_2 on Ge surface:* When left in atmosphere an unstable native oxide (GeO_2) forms on the surface of Ge. We can find in the literature [25] that GeO_2 fibres have a very high loss of 340-900 dB/cm in this range. If we assume the same loss in the GeO_2 film on the surface, and we assume that the film thickness is 20 nm, then simulations predict mode overlap with this film of 0.1%, and a maximum accompanying material loss of 0.09 dB/cm. This appears to be too small to cause the observed loss, but more data on the Ge native oxide infrared absorption would be desirable.

Optics EXPRESS

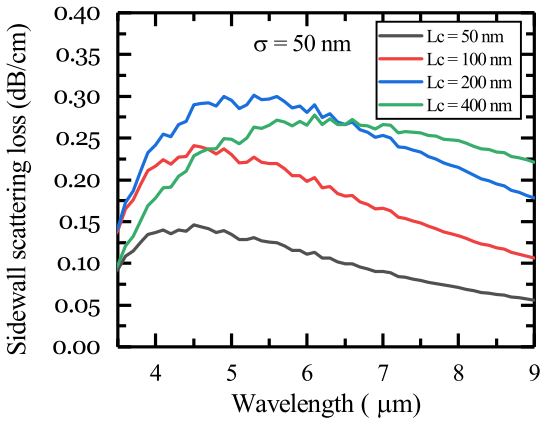

Fig. 7. Estimated Ge-on-Si waveguide loss from sidewall roughness scattering, with an r.m.s roughness (σ) = 50 nm, and varying correlation length (Lc).

e) *"Time dependent haze" (TDH) formation:* Looking to the SEM image in Fig. 3(b), it is apparent that there are imperfections on the Ge surface. Atomic force microscope measurements confirm that these are "mounds" of approximately 2 μm diameter that appear over time, and are the result of a process that begins with native oxide formation, and is assisted by moisture formation at the wafer surface [26]. It has been shown that this process can be mitigated through careful wafer storage that reduces moisture formation [26]. Nevertheless, the wafers used in this experiment were more than 6 months old when tested, so a high defect density is visible. These defects should increase the scattering loss, however the strong wavelength dependence of the loss is inconsistent with scattering. As previously stated, Rayleigh scattering has a λ^{-4} dependence, and we have simulated that the mode confinement in a 400 nm thick area centered along the Ge/air interface increases only from 5.0% to 7.0% over 7.5 μm to 8.5 μm. Therefore scattering loss at these defects is unlikely to be responsible for the large change in loss in the range. However, since the "mounds" are composed predominantly of GeO_2, which has high absorption, it is possible that a wavelength dependent loss of the material making up these mounds may be responsible.

f) *Ge interstitial oxygen or carbon:* As in Si, interstitial oxygen content can increase absorption in Ge, and indeed oxygen may be present in the Ge layer. A literature search shows that in Ge the absorption peaks from this effect manifest at < 875 cm^{-1} (i.e. > 11.4 μm) [27], therefore it is unlikely to be responsible for the high absorption seen here.

g) *Multiphonon absorption in Si and Ge:* Multiphonon absorption is responsible for the increased absorption in Si above ~8 μm [28] and in Ge above ~14 μm [29]. We speculate that a potential explanation for the waveguide loss increase could be a shift of the multiphonon absorption to lower wavelengths, caused by strain in the Ge film due to the Ge/Si lattice mismatch and differing thermal expansion coefficients in the two materials. A tensile strain of 0.13% was measured in the Ge layer using a KLA Tencor wafer stress measurement tool. To our knowledge there is no existing investigation of the Si and Ge multiphonon absorption dependence on strain, and we are unable to quantify it, therefore this hypothesis should be explored further.

h) *Free-carrier absorption:* Free-carrier absorption is the absorption due to the presence of electrons and holes, and is normally considered to be negligible in Si or Ge wafers unless they have been highly doped. However, in Ge free-carrier absorption is greater

Optics EXPRESS

than in Si [30], and also increases strongly with wavelength, such that its effect should be considered. We do not have data for the dopant concentration in the Ge layer, but the Ge was grown on p-type Si substrates with 5-20 Ohm.cm resistivity (equating to 2.3-7.6 x10^{14} cm^{-3} carrier concentration [31]). If we assume that the Ge layer has the same p-type doping of 7.6x10^{14} cm^{-3} as the Si substrate, we can estimate from [30] an accompanying loss of 1.4 dB/cm at 7.5 μm and 2.1 dB/cm at 8.5 μm. Both the level of this loss and the relative loss increase across the wavelength range are lower than in the experiment. Nevertheless, the free-carrier loss predictions in [30] have yet to be verified experimentally in this range, so may underestimate the effect, and the actual impurity concentration in the waveguide layer is unknown. Furthermore, the free-carrier absorption predictions were made for unstrained Ge, and may not be accurate for the strained Ge used here. It is clear that the very strong Ge free-carrier absorption in this range can be significant even at background doping concentrations that are considered negligible in Si and in the near-infrared. N-type Si exhibits lower free-carrier absorption than p-type Si, therefore using a n-type or high purity Si substrate for the growth would be expected to somewhat reduce the loss.

In this initial analysis none of the considered effects fully account for the high observed waveguide loss difference across the measured range. Absorption from the Si substrate and defect scattering effects do not appear to be responsible. At this stage, the most likely candidates seem to be the free-carrier loss from background doping of the Ge, or absorption at the Ge surface, either from native oxide formation or from time dependent haze. Further experimental investigation is critical in order to determine which effects are dominant in practice, so that strategies for minimising these losses can be developed, and to enable low loss Ge waveguides at wavelengths beyond 8 μm.

7. Conclusion

We have designed, fabricated, and optically characterized germanium on silicon waveguides operating in the 7.5-8.5 μm wavelength range. The propagation loss was measured by creating a "cut-back" loss circuit into which light is launched through a diced waveguide facet, the light is split into 8 waveguides of different lengths, and grating couplers defined at the end of each waveguide transmit light up towards an infrared camera, which simultaneously monitors the transmissions of all 8 waveguides. This measurement resulted in a minimum loss of 2.5 dB/cm at 7.575 μm, increasing to nearly 20 dB/cm at 8.5 μm. We conducted a literature review to identify potential sources of this loss increase, but initial estimates indicate that none of the considered loss mechanisms fully account for the observed effect. Therefore, further thorough experimental investigation is required, in order to identify what causes this loss and how it can be reduced.

Funding

Engineering and Physical Sciences Research Council (EPSRC) MIGRATION project (EP/L01162X/1); Royal Society Research Fellowship; European Research Council (ERC) grant "Wideband Integrated Photonics for Accessible Biomedical Diagnostics" (291216).

Acknowledgments

The data from this work is available online in the repository at https://doi.org/10.5258/SOTON/D0250.